A Punctuated Equilibrium Analysis of the Climate Evolution of Cenozoic: Hierarchy of Abrupt Transitions

Denis-Didier Rousseau, Witold Bagniewski, Valerio Lucarini

Science Advances
Manuscript Template

FRONT MATTER

Title

- Full title: A Punctuated Equilibrium Analysis of the Climate Evolution of Cenozoic: Hierarchy of Abrupt Transitions
- Short title: Hierarchy of Transitions in the Cenozoic

Authors

Denis-Didier Rousseau[1,2,3 *], Witold Bagniewski[4], Valerio Lucarini[5,6],

Affiliations

[1] Université Montpellier, Géosciences Montpellier, Montpellier, France
[2] Silesian University of Technology, Institute of Physics-CSE, Division of Geochronology and Environmental Isotopes, Gliwice, Poland
[3] Columbia University, Lamont Doherty Earth Observatory, New York, USA
[4] Ecole Normale Supérieure – Paris Sciences et Lettres, Laboratoire de Météorologie Dynamique, Paris, France
[5] University of Reading, Department of Mathematics and Statistics, Reading,
[6] University of Reading, Centre for the Mathematics of Planet Earth, Reading, UK

(*) corresponding author: denis-didier.rousseau@umontpellier.fr.

Abstract

The Earth's climate has experienced numerous critical transitions during its history, which have often been accompanied by massive and rapid changes in the biosphere. Such transitions are evidenced in various proxy records covering different timescales. The goal is then to identify, date, and rank past critical transitions in terms of importance, thus possibly yielding a more thorough perspective on climatic history. To illustrate such an angle, which inspired the punctuated equilibrium angle on the theory of evolution, we have analyzed 2 key high-resolution datasets: the CENOGRID marine compilation (past 66 Myr), and North Atlantic U1308 record (past 3.3 Myr). By combining recurrence analysis of the individual time series with a multivariate representation of the system based on the theory of the quasi-potential, we identify the key abrupt transitions associated with major regime changes that differentiate various clusters of climate variability. This allows interpreting the time-evolution of the system as a trajectory taking place in a dynamical landscape, whose multiscale features are associated with a hierarchy of tipping points.

Teaser

A hierarchy of Tipping Points shaped the Cenozoic: the time evolution of the system can be understood as a motion in a multiscale dynamical landscape

MAIN TEXT (The manuscript should be a maximum of 15,000 words)

INTRODUCTION

Early evidence of abrupt transitions in Camp Century and Dye 3 Greenland ice cores (*1*, *2*) attracted a lot of attention from the paleoclimatic community before being well acknowledged and understood. They have indeed introduced the evidence of a sequence of abrupt climatic variations that at the time were unknown. Nonetheless, such transitions did not seem to find an agreement with other marine and terrestrial records, which led to considerable debate in the field (*3–5*). After decades spent retrieving and studying more detailed paleorecords, the evidence for such rapid climatic variations, named Dansgaard-Oeschger events (DO), has been well accepted since then. They have been recently reinforced by the identification of additional abrupt transitions from the NGRIP ice core, which have been made possible by the increased time-resolution of the record (*6*). These additional events correspond to changes of either short duration or amplitude in δ^{18}O that visual or standard statistical inspections do not necessarily flag. The Earth climate has experienced numerous abrupt and critical transitions during its long history, well beyond the specific examples above (*7*, *8*). Such transitions are often referred to as climatic tipping points (TPs), associated with possibly irreversible changes in the state of the system. The term TP was originally introduced in social sciences (*9*) and made more recently popular thanks to (*10*). The study of TPs has recently gained broad interest and perspective in Earth and Environmental sciences, especially with regard to the future of our societies under the present climate warming scenarios (*11–14*). The term Tipping Elements (TE) was introduced by (*13*, *15*), and subsequently adopted by others (*12*, *16*) to characterize the particular components of the Earth System that are likely to experience a TP in the near future (*14*, *17–19*). Recently, the concept of TP has been used to define, in turn, rapid societal changes that might lead to positive impacts in terms of addressing the climate crisis (*20*, *21*).

Here, we want to investigate critical transitions in the Earth history by looking at 2 key high-resolution datasets that show evidences of abrupt transitions. The first dataset is the CENOGRID benthic δ^{18}O and δ^{13}C record corresponding to the compilation of 14 marine records over the past 66 Myr, from the Cretaceous-Paleogene (K–Pg) extinction event till present (*22*). The second dataset comprises the North Atlantic U1308 benthic δ^{18}O, δ^{13}C and δ^{18}bulk carbonate time series covering the past 3.3 Myr (*23*).

While visual evidences of abrupt transitions have already been discussed for these datasets, we wish to identify key abrupt thresholds by applying the recurrence quantification analysis (RQA) to the individual time series and supplementing it with the Kolmogorov-Smirnov (KS) test (*24*), see below. Then, the selected transitions are discussed in the context of the Earth climate history allowing the definition of dynamical succession of abrupt transitions. Such transitions are then interpreted taking into account the evolution of key climate factors such as CO_2 concentration, average global sea level, and depth of the carbonate compensation.

The existence of TPs is intimately related to the multistability properties of the climate system, which have long been recognised in different contexts; see e.g. (*25–28*) and discussion in (*29*) and (*30*). The multistability of the climate system is associated with the presence of more than one possible climate states for a given set of boundary conditions (*31*). While earlier analyses have mostly evidenced the possibility of bistable behaviour, multistability can indeed include multiple competing states (*32–35*). Recently, it has been proposed that the metastability properties of the climate system can be understood by taking a different angle that, rather than focusing on the actual succession of TPs, interprets the climate evolution as a diffusion process taking place in an effective dynamical landscape (*36*, *37*), the Graham's quasi-potential (*38*). Such a viewpoint mirrors earlier proposals for interpreting biological evolution, namely the Waddington's epigenetic landscape (*39–43*), and foresee the rapid climatic transitions associated with the TPs as a manifestation of a dynamics characterized by punctuated equilibria (*44*, *45*); see also relevant literature associated with synthetic evolution models like Tangled Nature (*46*, *47*). We will test whether the RQA identifies candidate TPs that come hand in hand with saddles of the quasi-potential, and whether TPs featuring faster characteristic time scales are associated with smaller-scale decoration of the quasi-potential (*36*). The analysis of the benthic $\delta^{18}O$ and $\delta^{13}C$ suggests that the evolution of the climate in Cenozoic is characterized by a hierarchy of TPs due to an underlying multiscale quasi-potential.

RESULTS

Detecting Critical Transitions of the past 66 Myr – 3 Myr history of the Earth Climate

The KS augmented test of the benthic $\delta^{18}O$ record of the past 66 Ma identifies seven major abrupt transitions corresponding to two major warming events at about 58 Ma and 56 Ma, followed by five major coolings at 47 Ma, 34 Ma, 14 Ma and 2.8 Ma respectively (Fig. 1A). Such transitions are characterized by a long-time scale in terms of permanence in the competing states (a long time-window of 1-4 Ma is used, see Suppl. Mat.). These events are classical ones described from the literature (*48*), where the first two transitions led to warmer conditions, while the latter four led to colder conditions. The same transitions are identified by employing the recurrence plot (RP) and recurrence rate (RR) analyses (*49*), which also identify two more events, occurring at around 63 Ma, 20 Ma, and 9.7 Ma, see Fig. 1C, Suppl. Tab. 1. We have chronologically labeled these TP_O1 to TP_O9, where the lower index refers to the used proxy data. As shown in Fig 1B, TP_O5 separates the climate variability in two separate macroclusters prior and after 34 Ma, the well-known Eocene-Oligocene Transition (EOT) (*50*), which is a key step in the Cenozoic climate history and is associated with a major extinction event (*51*, *52*).

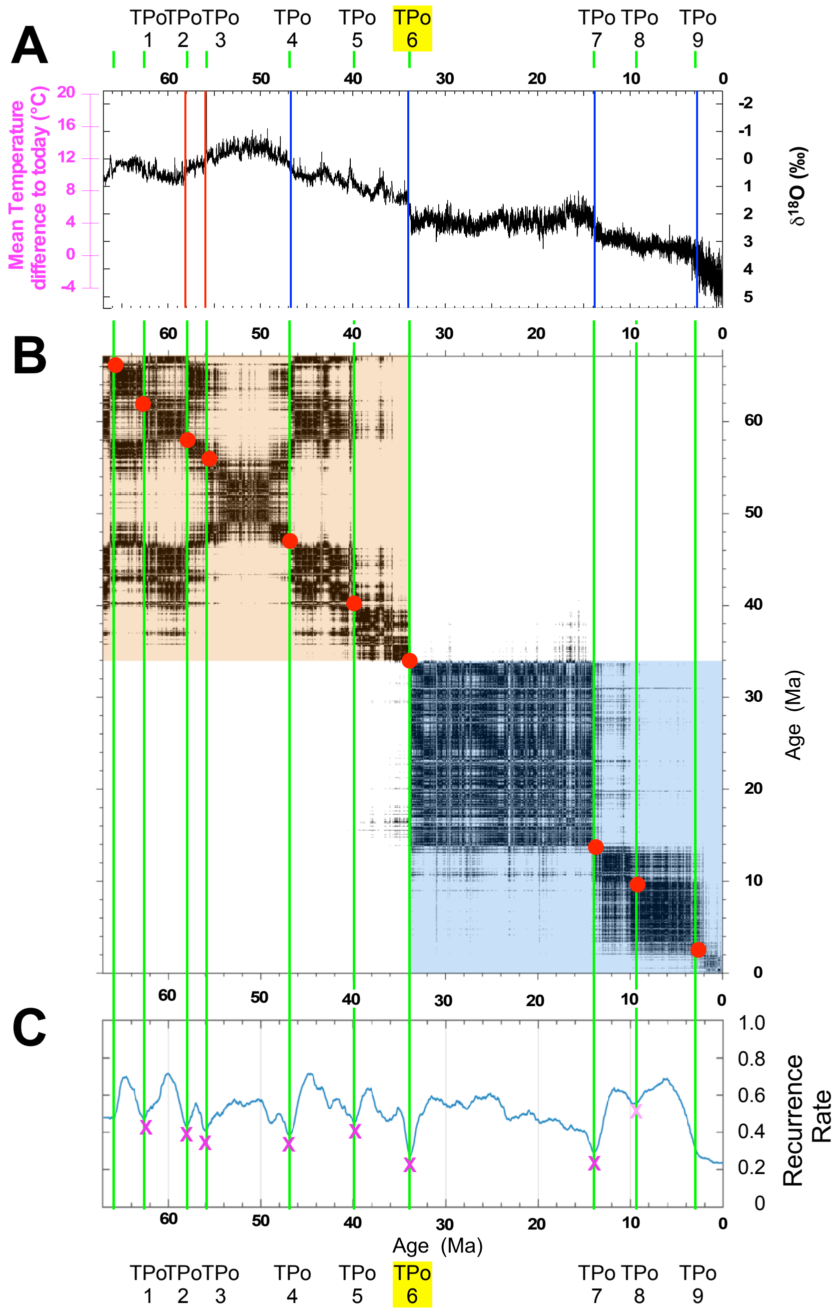

Fig. 1. **KS test and Recurrence Quantitative Analysis (RQA) of CENOGRID benthic δ^{18}O.** A) Time series in Ma BP with difference of the reconstructed and present Mean Global Temperature in pink). KS test identifying abrupt transitions towards warmer conditions in red and cooler or colder conditions in blue; B) Recurrence plot (RP) with identification of the main two clusters prior and after 34 Ma. The main abrupt transitions identified are highlighted by red circles, and C) Recurrence rate (RR). The pink crosses and vertical green lines indicate the abrupt transitions (TP_O) detected by the RQA. CENOGRID benthic δ^{18}O data are from (*22*)

The older macrocluster shows a disrupted variability, according to Marvan et al.'s nomenclature (*49*). One finds very large negative values of the benthic $\delta^{18}O$, which correspond to the very warm climate conditions. The average global temperature was estimated to be between 8°C and 16°C above the present day one, with no apparent presence of any major continental ice bodies (*22*) (Fig. 1A). Four major transitions are found within this period. They include the 2 major abrupt warmings at 58 Ma (TP_O2) and 56 Ma (TP_O3). These two transitions correspond to thresholds towards much warmer oceanic deep water corresponding to the first late Paleocene-Eocene hyperthermal (*53, 54*) and Paleocene-Eocene Thermal Maximum (PETM) (*55, 56*) respectively. The third one at about 47 Ma (TP_O3) corresponds to a transition towards cooler deep waters and named the Early-Middle Eocene cooling (*54*). The last one at about 40 Ma (TP_O4) inaugurates the period of continuous cooling due to decrease of CO_2 concentration that eventually leads to the TP_O6 event (*57*), which leads to the build-up of the Antarctica ice sheets. TP_O5 clearly separates two fundamentally different modes of operation of the climate system. From 34 Ma to present day the records features more positive values of benthic $\delta^{18}O$ associated with prevailing colder climate conditions. After TP_O6, the climate featured mostly stationary conditions with a slight warming until the Middle Miocene Climate Transition (TP_O7) that occurred around 14 Ma (*58*, *59*). The last major transition (TP_O9) occurred around 2.8 Ma, leading to the Pleistocene and the onset of glaciations in the Northern Hemisphere.

In this work, we will prioritize the information coming from the $\delta^{18}O$ record because of its very strong link to the Earth's temperature. Nonetheless, the analysis of the Benthic $\delta^{13}C$ record performed along the same lines as above provides separate pieces of information on the critical transitions of the Earth's Climate. Benthic $\delta^{13}C$ values characterize deep-water ventilation with high $\delta^{13}C$ values in regions close to deep-water formation area. The KS analysis performed over a time window of 1-4 Myr individuates 14 TPs, with the RP suggesting an additional one, located at around 34 Ma and associated with the EOT. We refer to these 15 TPs associated with the $\delta^{13}C$ record as TP_C 1 to 15; see Suppl. Fig. 1, Suppl. Tab. 1. The interval 56.15 Ma – 7.15 Ma is well characterized, showing some subclusters distributed around 34 Ma. The 56.15 Ma date groups $\delta^{13}C$ values above 1‰, at the base of the record, while 7.15 Ma gathers the negative $\delta^{13}C$ values which mainly occurs on top of the record. The two periods are characterized by very different climatic conditions. The earlier climate regime features more input of carbon in the ocean while the later climate, instead, is characterized by higher presence of carbon in the atmosphere.

Critical Transitions in other Proxy Data

We next want to analyze TP_O 1-9 in relation to different reconstructed paleoclimatic data, namely the global mean sea level (GMSL), the Pacific carbonate compensation depth (CCD), and CO_2 concentration (Fig. 2). Using benthic foram $\delta^{18}O$ and Mg/Ca records from high-resolution Pacific cores different from CENOGRID ones, (*54*) have reconstructed the variations of the GMSL of the past 66 Ma. Measuring the carbonate content in sediment Pacific cores and applying transfer functions, (*60*) have computed a detailed Cenozoic record of the Pacific CCD below which carbonates dissolve. Finally, compiling estimates from various proxies including foram $\delta^{13}C$, boron isotopes, stomata, paleosols. (*61*) have released a comprehensive Cenozoic record of the CO_2 concentration. One clearly observes the signature of the TP_O6 in the three records, as it corresponds to an abrupt decrease of the GMSL by about 70m and of the CCD by around 1000m. Additionally, TP_O6 signals the start of the progressive decrease of the CO_2 from values of the order of 750 ppm to values of the order of 280 ppm.

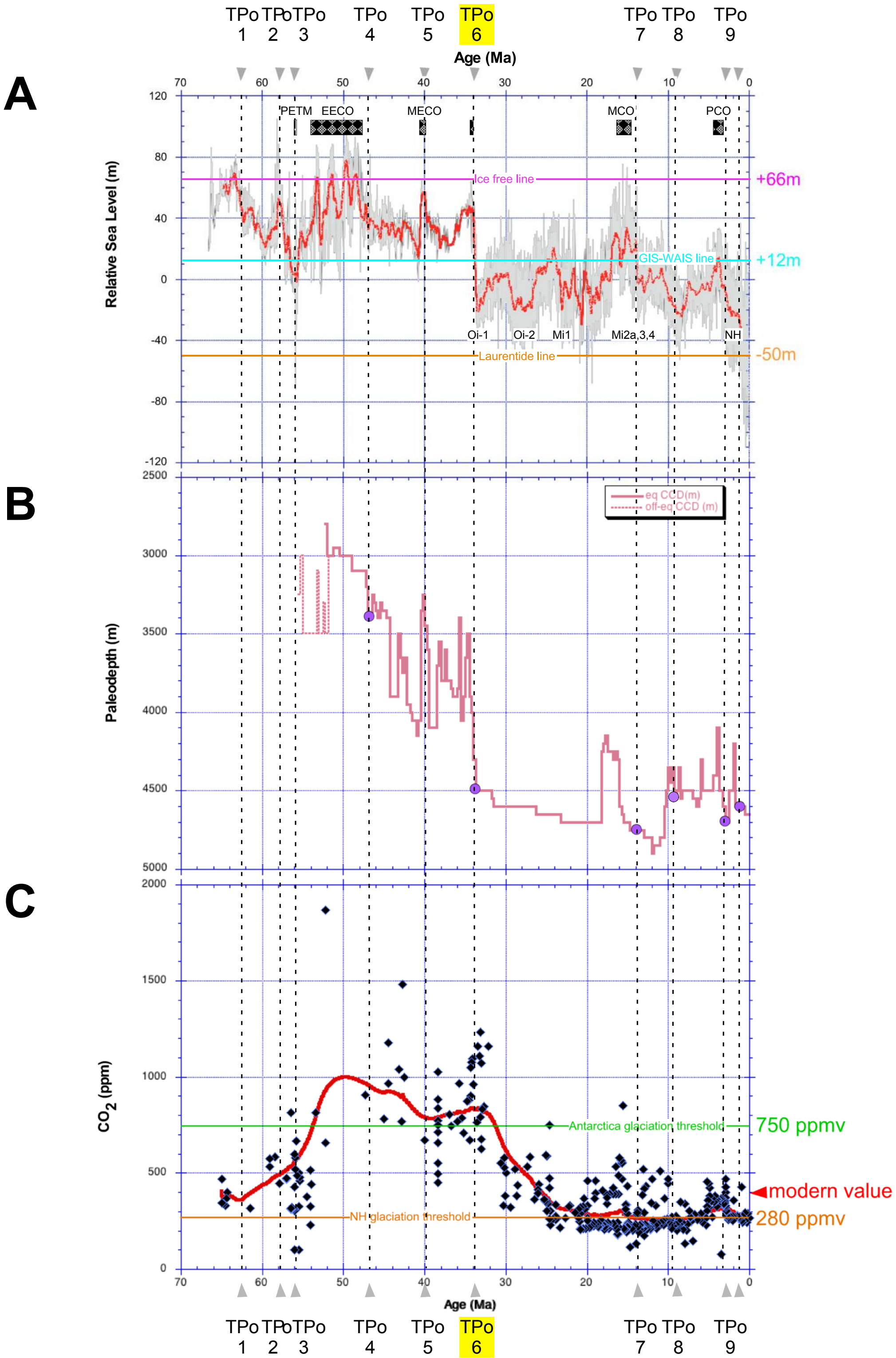

Fig. 2. **Variation through time of three main climate factors and comparison with the identified abrupt transitions (TP) in the CENOGRID benthic δ^{18}O.** A) Global Mean Sea Level in meters from (*54*). Identification of specific warm and of glaciation events. The Laurentide, GIW-WAIS and Ice free lines are from (*54*); B) Carbonate Compensation Depth (CCD) in meters from (*60*). The purple circles identify the TPs on this record; C) Estimate of the CO_2 concentration in parts per million volume (ppmv) from (*61*). The Antarctica glaciation threshold at 750 ppmv and the NH glaciation threshold at 280 ppmv lines respectively are from (*62*)

One can identify four competing states,"Warmhouse" (66 Ma-TP$_O$1 and TP$_O$3- TP$_O$5) and "Hothouse" (TP$_O$1-TP$_O$3) climates in the earlier, warmer period, followed by the "Coolhouse" (TP$_O$5-TP$_O$6) and "Icehouse" climates (TP$_O$6 to present); see Fig. 1.

The first two states alternated in a warm-hot-warm sequence under extremely high CO_2 concentrations (*61*) as compared to those measured over the past 800 Kyr in the Antarctic ice cores, which represent the reference states for the IPCC potential scenarios of climate change warming (*63*) (Fig. 2C). Before 34 Ma, one finds substantially larger values for GMSL, CCD depth, and CO_2 concentration whose average values are: +38 ± 15 m, 4600 ± 150 m, and 630 ± 300 ppmv respectively (Suppl. Tab. 2). Note that the CO_2 concentration is much higher than what observed in the past 800 kyr in the Antarctic ice cores, which represent the reference states for the IPCC potential scenarios of climate change warming (*63*). Conversely, from 34 Ma until present, under much lower CO_2 concentrations and GMSL, thus generating the classical climate trend towards the recent ice-age conditions (*8*, *22*, *48*) (Fig. 2A,C). Indeed the last 34 Myr show average values in GMSL, CO_2 concentration and CCD depth of -3.5 ± 13 m, 330 ± 160 ppmv and 3500 ± 400 m respectively (Tab. 2), which are much lower than in the older interval. This second set of means are underestimated values because the final values of (*54*) dataset ending at 0.9 Ma,

These GMSL, CCD and CO_2 reconstructions show key transitions that fit with the CENOGRID thresholds deduced from the KS and RR analysis of the benthic $\delta^{18}O$ as they signal increase or a decrease in the global mean sea level corresponding roughly to warming or cooling episodes of the Earth history or strong variations in the concentration of atmospheric CO_2. The variations observed in CO_2, CCD and GMSL at the 9 identified TPs from the benthic $\delta^{18}O$ record indicate heterogeneous characteristics prior to the TP6 major threshold (Suppl. Tab. 3). On the contrary, more homogenous features are noticed in the three climate proxies after TP_O6, translating the occurrence of major reorganizations in the climate system, which become interesting to test at shorter timescales; see discussion below.

A Historical Account of the Critical Transitions

Added to the Chicxulub meteor impact previously mentioned, which injected a considerable amount of CO_2 into the atmosphere (*64*, *65*), Deccan traps were already spreading at the beginning of the Cenozoic, contributing to the release of massive amount of CO_2 (*8*). CO_2 concentration continued raising until about 500 ppmv with the North Atlantic Igneous province very active at about 58 Ma – 56 Ma (TP_O2 and TP_O3) in relation with the opening of the North Atlantic Ocean (*66*). The Northern Hemisphere plates were connected and not facing the present Arctic conditions allowing faunal and vegetal dispersion. Other plates were on the contrary reorganizing like India moving northeastward toward the Asian continent. Equatorial Pacific carbonate compensation depth (CCD) reached a minimum value a bit later at about 54 Ma when CO_2 concentration reached its maximum of the whole Cenozoic above 1,100 ppmv (*61*). The lowering of the GMSL and of the CCD at TP_O4 (about 40 Myr) has been interpreted as the start of the icing of Antarctica through mountain glaciers deposits dates by K-Ar dating of lava flows (*67*), supported by other glacial evidences i.e., from the Gamburtsev subglacial mountains (*68*), while Northern Hemisphere plates remained connected. By TP_O4 India is approaching the Asian plate while Northern Hemisphere ones were still connected, allowing northern continental migrations of mammals at high latitudes (*69*, *70*). About 34 Ma, the EOT (TP_O6) is associated with the opening (in several steps) of the Drake and Tasmanian passages (*71*), which lead to a drastic change in the global ocean circulation. The effect is a decrease in the South Hemisphere water formation strength, a deep-sea temperature drop associated with the deep fall in relative sea level and CCD (see Fig. 2). According to paleoaltimetry estimates based on oxygen isotopes, (*72*) indicate that the Tibetan Plateau had an elevation of about 4000m, favoring therefore the physical weathering of rocks, consuming CO_2, and the burial of carbon through high sedimentation rates in the adjacent seas. This may have contributed to the major threshold in the variation of the CO_2 concentration, which also drops very strongly ((*61*); Fig. 2).

This key transition is the major boundary between two different climate landscapes dominated by intensive plate tectonic and major volcanism for the older one, and by major ice sheets in both Southern and Northern Hemispheres, with plate tectonic (closure of seaways, orogenies) still very active, for the younger one (*70*). Immediately after the EOT, the climate witnessed the build-up of the East Antarctic ice sheet (Oi-1 glaciation), which can be considered as the onset of the cold world in which we are still living. India has almost ended its transfer to the Asian plate. Between TP_O 6 and TP_O 7, i.e., 34 Ma and 14 Ma respectively, the East Antarctic ice sheet is waxing and vanning with several major glaciations occurring before the 17 Ma to 14.5 Ma interval during which sea level increases in association with a severe shoaling episode of CCD and higher values of the CO_2 concentration (Fig. 2). Such high CO_2 concentrations may have been fueled by the Columbia River major volcanism, which ended by TP_O 7 at about 14 Ma (*8*). Plate tectonics is still very active with the closure of both the Indonesian gateway and the Tethyan seaway, contributing to the start of the development of the Mediterranean (*73*), and. Eurasia is now separated from Northern America and Greenland, India colliding the Asian continent, and the Andes are uplifting modifying the geometry of the marine basins and the global oceanic circulation. West Antarctica is starting building up while East Antarctic ice sheet is reinforcing and expanding. TP_O8 at about 9 Ma sees a strong lowering of the GMSL and of the CO_2 concentrations (Fig. 2). TP_O9 is associated with a final major tectonic event corresponding to the closure of the Panama Isthmus, which as a result of shutting down the exchange of water between the two oceans, led to re-routing large-scale flows in both the Pacific and the Atlantic Ocean, and configured a oceanic circulation that is very similar to present day (*74*). This is associated to a strong lowering of the global sea level, a deepening of the CCD and the CO_2 concentration (Fig. 2) that will preside the Earth climate history during the Quaternary, associated to the build-up of the Northern Hemisphere glaciers and ice sheets. It is interesting to notice that all the major transitions that have been identified during the interval between 66 Ma and 2.9 Ma - 2.5 Ma are linked to the build-up, waxing, and vanning of the Northern and Southern Hemisphere ice sheets.

Quasi-potential Landscape and Critical Transitions

As discussed in detail in the Methods section, taking inspiration from the use of the Waddington epigenetic landscape to describe evolution (*39–43*) and from the theory of punctuated equilibrium (*44*, *45*), it has been proposed in (*36*, *37*) to study the global stability properties of the climate system by introducing an effective quasi-potential (*38*), which generalizes the classical energy landscape framework often used to study metastable stochastic system. The quasi-potential formalism allows one to study general nonequilibrium system and to associate local maxima of the probability distribution function (pdf) of the system stable states. Additionally, saddles of the pdf are associated with Melancholia (M) states (*31*), which are unstable states living in the boundary between different basins of attraction. In the weak-noise limit, noise-induced transitions between competing stable states are expected to go through such M states. What we have done here is to construct the empirical bivariate pdf of climate system in the projected ($\delta^{13}C$, $\delta^{18}O$) and check whether TP_O 1-9 indicated in Fig. 1 correspond, at least approximately, to saddles of the pdf. We find – see Fig 3A – that, indeed, this is the case of TP_Os 1, 2, 4, 5, 6, 8, 9, whereas no agreement is found for TP_Os 3 and 7, which seem to take place in regions where the density is very small and very large, respectively. The pdf shown here had already been used in (*22*) to identify the Icehouse, the Coolhouse, the Warmhouse, and the Hothouse states. Our angle here, instead, allows to better identify the transitions between such states, and the special role played by TP_O6, which basically breaks the pdf into two separate parts. Note that the transitions shown in Fig. 1 are associated, because of the choice of a long time-window, with events that occur over long periods and that lead to persistent changes in the state of the system.

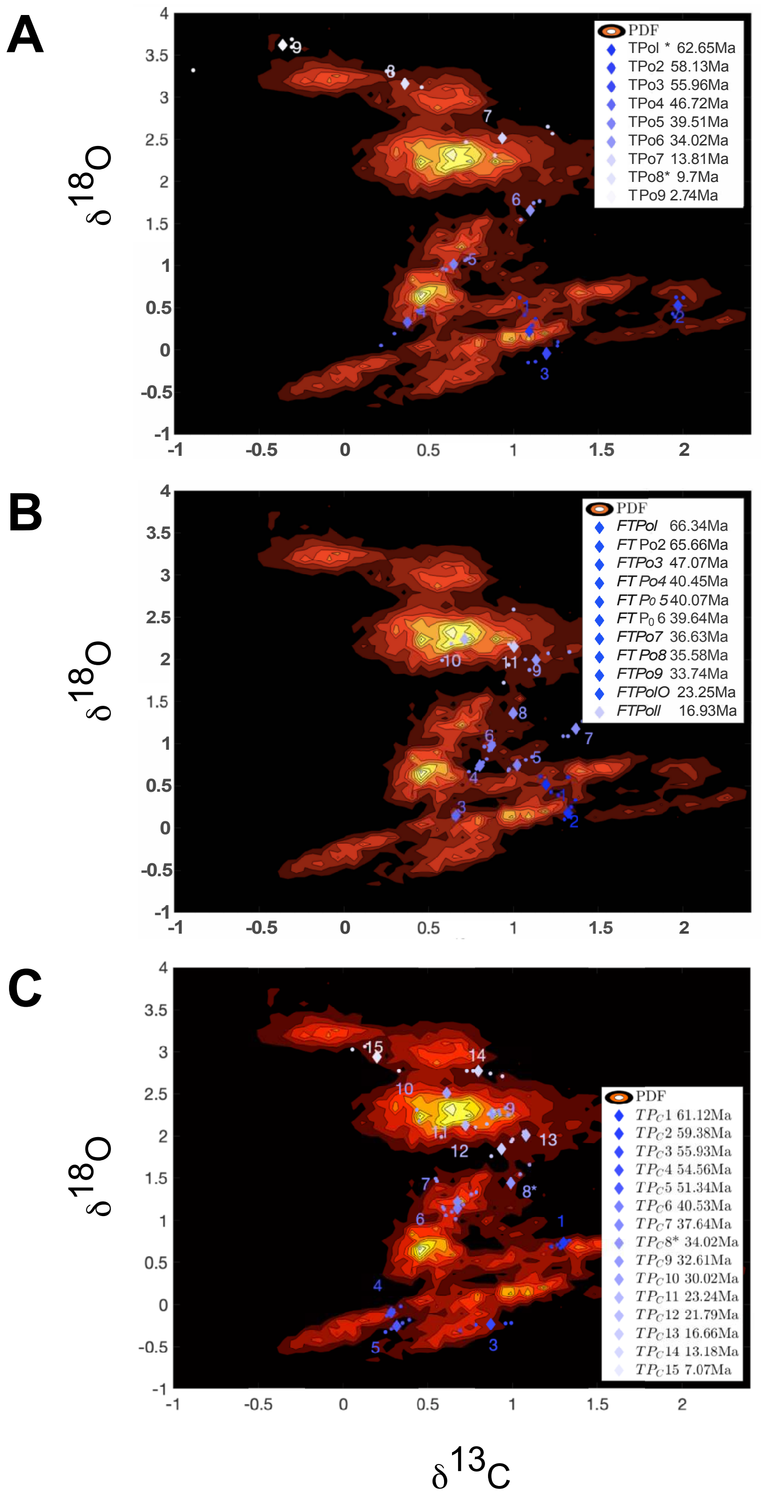

Fig. 3. **Probability density of the climate system in the projected CENOGRID benthic δ^{18}O and δ^{13}C. space.** Panel a) Chronologically ordered TP_Os (diamonds) selected according to the KS methodology for δ^{18}O with time window 1-4 My are shown. The two extra TP_Os found via RP are indicated with a *. Panel b) Chronologically ordered fast TP_Os (FTP_Os, diamonds) selected according to the KS methodology for δ^{18}O with time window 0.25-1 Myr are shown. Panel c) Same as a), but for the δ^{13}C record. The approximate timing of the TPs is indicated (rounded to .01 My). The 5 Ky-long portions of trajectories before and after each TP are also plotted.

It is natural to ask ourselves what happens if, instead, we consider a catalogue of transitions for the δ^{18}O record that are detected by considering shorter time windows (0.25 Ma-1Ma) in the KS procedure. One finds – see Fig. 3B - 11 of such transitions (see Suppl. Mat.). Once we report such fast TP_Os (FTP_Os) into the empirical bivariate pdf of the climate system in the projected ($\delta^{13}C$, $\delta^{18}O$) space, we find that they correspond to finer and smaller structures of the pdf as opposed to the case of the TPs. Hence, events that are associated with faster time scales are associated with smaller jumps between secondary maxima in the pdf belong to a hierarchically lower rung than those occurring over longer time scales. This seems to support the proposal made in Ref. (*38*).

As additional step, we repeat the same analysis leading to Fig 3A by using, instead, the $\delta^{13}C$ record, which features, as mentioned above, a total of 15 TP_Cs. Figure 3C shows clearly that the TP_Cs correspond for the most to saddles that had not been flagged by the TP_Os. We have evidence that the same saddle is crossed more than once in a back-and-forth fashion few millions of years apart (e.g. TP_C s 4 & 5; TP_Cs 6 & 7; TP_Cs 12 & 13), which supports the dynamical interpretation discussed here. Comparing Figs 3A and 3C, one discovers that the same saddle is responsible for TP_O8 and for TP_C15 even if the dating is different. Similarly, the same saddle is responsible for TP_O5 and TP_Cs 6 & 7. Two key climatic features that appear as TPs in both records: the PETM corresponds to TP3 in both records, while the EOT corresponds to TP_O6 and TP_C8.

The recent past

The past 3.3 Myr record from North Atlantic core U1308, can be considered as a blow-up of the CENOGRID dataset (Fig. 4). As previously mentioned, the last 3.3 Myr have been defined as an Icehouse climate state, with the appearance, development, and variations of the NHIS (*22*), with the Antarctic ice sheets already reached mostly their maximal expansion. The variations in the deep-water temperature, as expressed by the benthic $\delta^{18}O$, are interpreted as an indicator of the continental ice volume with clear interglacial-glacial successions (*75*–*77*). The Icehouse state is characterized by a change of the interplay between benthic $\delta^{13}C$ and $\delta^{18}O$, which corresponds to a new relationship between the carbon cycle and climate (*78*). Indeed, one finds a very strong correlation between the two records (Pearson's coefficient being approximately -0.6). The correlation mainly results from the fact that the time series have approximately a common quasi-periodic behaviour due to resonant response to the astronomical forcing, as discussed below. Note that that the presence of such almost regular resonant oscillations makes the use of the quasi-potential framework not particularly useful for describing the dynamics of the system.

The KS augmented test and the RQ of the benthic $\delta^{18}O$ agree in identifying six abrupt transitions dated at approximately 2.93 Ma, at 2.52 Ma, at 1.51 Ma, at 1.25 Ma, at 0.61

Ma and at 0.35 Ma (Fig. 4, Suppl. Tab. 1). They characterize the dynamics of North Hemisphere ice sheets (elevation and spatial expansion) and agree with the classical transitions characterizing the Marine Isotope Stages (MIS) as already observed in numerous records covering the same interval (see (*79*) and Refs. therein).

The first two transitions broadly correspond with the previously discussed CENOGRID's TP_O9 associated with the onset of the Pleistocene (note that the interval between the two is much smaller than the resolution needed to separate to TP_Os) and are followed by four more recent TPs associated with the benthic $\delta^{18}O$ record (RTP_Os). There is clear evidence of the Mid-Pleistocene (MPT) critical transition, between 1.25 Ma and 0.8 Ma, during which a shift occurred from climate cycles dominated by a 40-kyr periodicity (due to obliquity) to 100-Kyr periodicity (due to eccentricity) dominated ones (*80–84*). The 1.25 Ma date is particularly significant, since it is followed by an Increase in the amplitude of glacial–interglacial fluctuations.

A complementary RQA of the $\delta^{18}O$ bulk carbonate record from U1308, which characterizes episodes of iceberg calving into the North Atlantic Ocean IRD released into the North Atlantic Ocean (*23*), and therefore illustrates the dynamics of the Northern Hemisphere ice sheets (NHIS), yields similar dates to those obtained for the benthic $\delta^{18}O$ record (see Suppl. Fig. 3, Suppl. Tab. 1) (*79*). Indeed, one finds abrupt transitions at 2.75 Ma, at 1.5 Ma, at 1.25 Ma, at 0.9 Ma and 0.65 Ma. Finally, as opposed to the CENOGRID $\delta^{13}C$ RP, U1308 $\delta^{13}C$ RP shows a drifting pattern similar to that of benthic $\delta^{18}O$, with only 2 key transitions at 2.52 Ma and 0.48 Ma (see Suppl. Fig. 3). Note that the 0.48 Ma transition does not have any equivalent in the benthic $\delta^{18}O$ records.

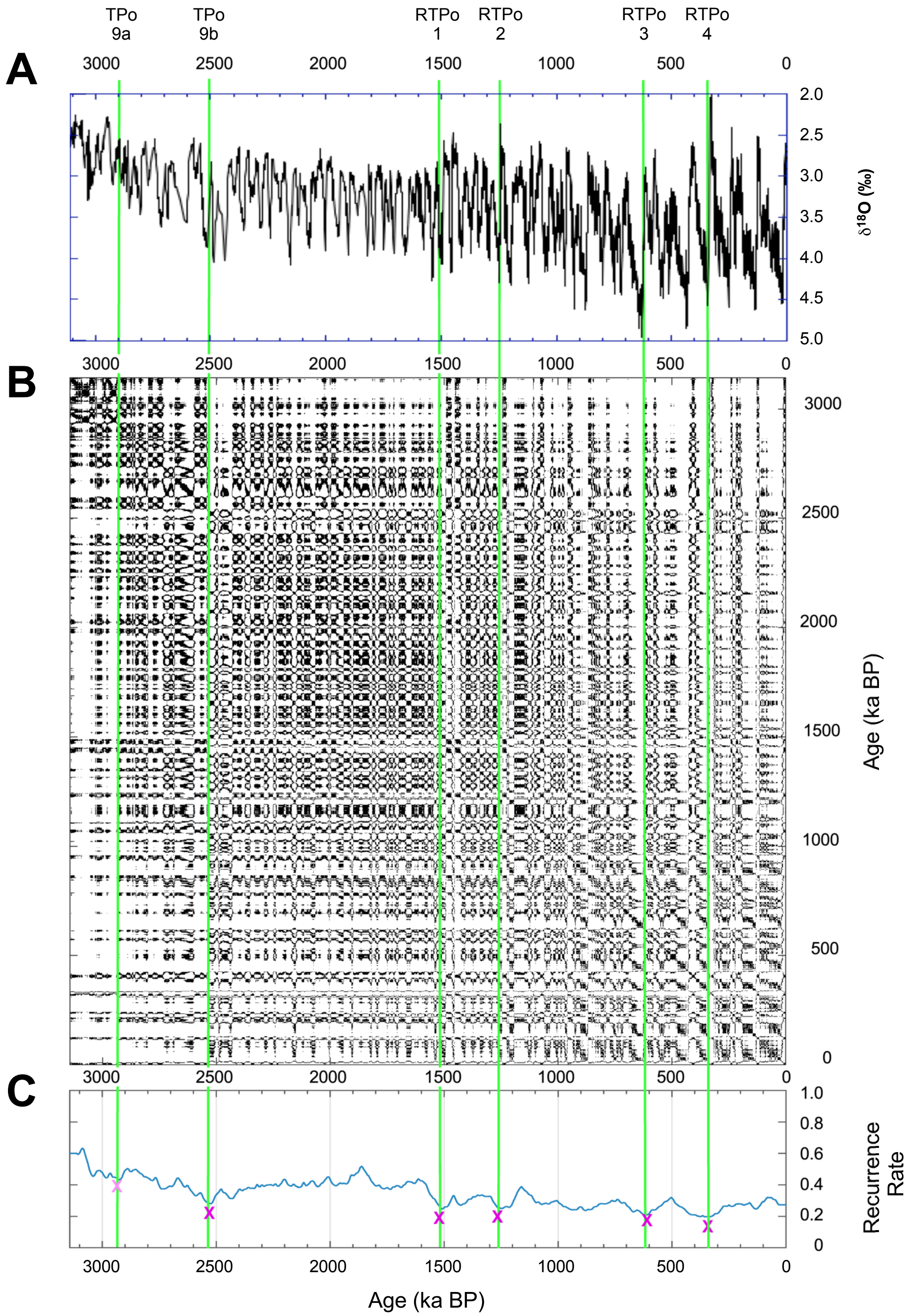

Fig. 4. **RQA of U1308 benthic δ^{18}O**. A) Time series in Ma; B) RP; and C) RR. Crosses similar than Fig. S1. TP_O9 and RTP_O1-4 abrupt transitions identified in the RR. U1308 benthic δ^{18}O data are from (*23*)

DISCUSSION

Studying the same CENOGRID dataset, Ref. (*85*) identified 9 geological transitions at respectively 62.1 Ma, 55.9 Ma, 33.9 Ma, 23.2 Ma, 13.8 Ma, 10.8 Ma and 7.6 Ma. Four of them are indeed identical to those determined in the present study: 62.1 Ma, 55.9 Ma, 33.9 Ma and 13.8 Ma, the first two being preceded by a significant early warning signal (*85*), which is instead absent in the case for the EOT key transition.

Considering the results of both RQA, KS test of the $\delta^{18}O$ and $\delta^{13}C$ time series considered in this study and the bivariate analysis performed using the framework of the quasi-potential theory, we propose a succession of critical transitions as described in Fig. 5. The critical transitions TP_O1 to TP_O9 shaped the Earth climate towards the onset and development of the Southern ice sheets and the later build-up of the NHIS. TP_O9 is followed by four more recent RTPs in the Quaternary, which steered the evolution of the ice sheets and of the climate as a whole until present day. The climatic evolution in the Cenozoic until about 3 Ma seem to conform to a punctuated equilibrium framework, where the TP_Os are associated with transitions between rather different modes of operation of the climate system. In particular, the key step that separates two rather diverse sets of climatic states occurred about 34 Ma at the EOT (TP_O6). Without the major drop in GMSL, in CO_2 concentration and in CCD, the Earth climate could have been different. However, after TP_O6, the Earth climate entered new dynamical regimes marked by much lower CO_2 concentration, lower GMSL and CCD. The oceanic basin redesign and the mountain uplifts changed the marine and atmospheric circulations patterns, leading to the onset and development of the NHIS.

Interestingly, the analysis of the $\delta^{13}C$ time series leads to identifying a different set of critical transitions – except for the case of the PET (TP_O2 and TP_CC) and the EOT (TP_O6 and TP_C8), which are recovered for both proxy data. Looking into the bivariate pdf in the projected ($\delta^{13}C$, $\delta^{18}O$) space allows to better understand the nature and the origin of the TPs separately detected by studying the recurrence properties of the univariate time series. Indeed, we are in most cases able to associate both the TP_Os and the TP_Cs to transitions across saddles of the effective quasi-potential. Clearly, some critical transitions might be better detectable when looking at one rather than the other time series, yet the angle taken here allows to put all TPs within a common ground. Additionally, TPs associated with faster processes and occurring between slower TPs correspond to transitions across smaller-scale saddles of the quasi-potential, hence revealing a correspondence between the hierarchy of TPs and the multiscale nature of the quasi-potential.

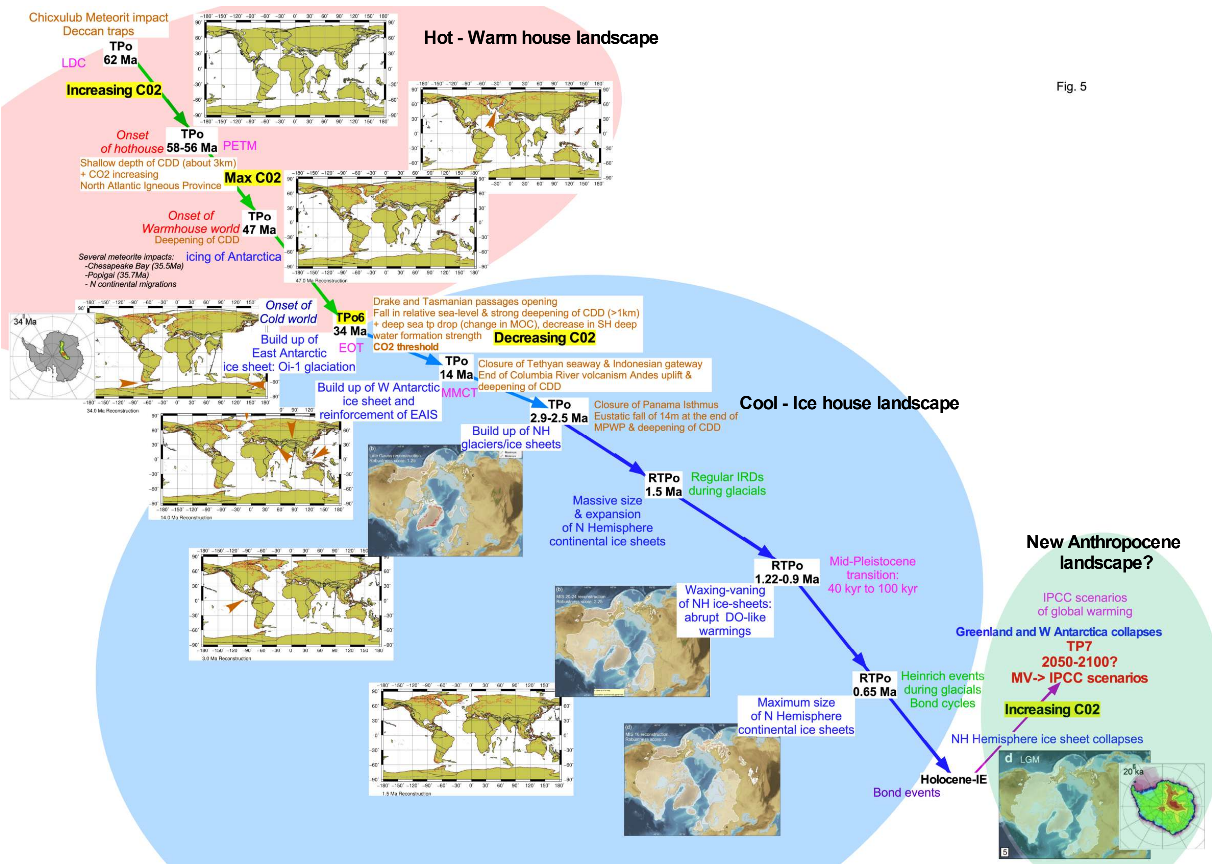

Fig. 5. **Evolution of the Earth Climate history among 2 different dynamical landscapes and proposal for a potential third one.** The first dynamical landscape in light red, corresponds to the Hot-Warm House time interval. The second dynamical landscape in light blue corresponds to the Cold-Ice house time interval. The third landscape, in light green, corresponds to the potential new one represented by the Anthropocene time interval. The different abrupt transitions identified in the present study are reported as TPos or RTPos to differentiate the major tipping points up to the early Quaternary period from the more recent TPs characterizing less drastic climate changes in the Quaternary. Various plate tectonic and ice sheet events are indicated and supported by maps of plate movements and North and South Hemisphere ice sheets. The Antarctica maps are from (*86*), Northern Hemisphere ice sheet maps are from (*87*). The paleogeographic maps have been generated using the Ocean Drilling Stratigraphic Network (ODSN) plate tectonic reconstruction service: < https://www.odsn.de/odsn/services/paleomap/paleomap.html>. The red arrows on the tectonic maps indicate the key events at the identified abrupt transition.

More recently, variations in the NHIS extent and volume have contributed to the occurrence of the millennial variability marked by the Bond cycles as better described during the last climate cycle but, which onset has been proposed to be dated of 0.9 Ma (*79*). Human activity is now rapidly pushing the Earth system towards the limits of its safe operating space associated with the occurrence of TPs. This concern is supported by actual observations impacting numerous tipping elements (see (*12*) through very drastic tipping cascades (*14*). This paves the way for a possible upcoming major transition, which might be fundamentally different from what observed in the recent or more distant past, and, at the very least, could bring us into in perspective into a climate state with much reduced or absent NHIS. Hence, we can foresee the possibility of the Earth system exploring a rather different dynamical landscape. This potential major transition, leading to de factor irreversible changes for the climate and the biosphere, could be the boundary between the Cenozoic icehouse and a new warmer and radically different climate state with respect to Pleistocene conditions.

METHODS

Recurrence Plots and Kolmogov-Smirnov Test

The augmented Kolmogorov-Smirnov test is a robust method for identifying discontinuities in a particular time series and is therefore a very precise way for timing the onset of abrupt transitions. It has been successfully applied to various geological time series (*24*, *79*, *88*). The method compares two samples taken before and after the potential transition point to test whether they come from the same continuous distribution. If they do not, the transition point is identified as a significant abrupt change indicative of a true climatic shift. (see for more details (*24*, *79*))

To gain further insight like recurring patterns into the climate story the records tell us, we performed a quantitative, objective analysis of these time series of proxy variables, based on the recurrence plots (RPs) introduced by (*89*) into the study of dynamical systems and popularized in the climate sciences by (*49*, *90*). The RP for a time series $\{x_i: i = 1, \ldots, N\}$ is constructed as a square matrix in a cartesian plane with the abscissa and ordinate both corresponding to a time-like axis, with one copy $\{x_i\}$ of the series on the abscissa and another copy $\{x_j\}$ on the ordinate. A dot is entered into a position (i, j) of the matrix when x_j is sufficiently close to x_i. For the details — such as how "sufficiently close" is determined — we refer to (*89*) and (*90*). All the points on the diagonal $i = j$ have dots and, in general, the matrix is rather symmetric, although one does not always define closeness symmetrically; to wit, x_j may be "closer to" x_i than x_i is to x_j (*89*). An important advantage of the RP method is that it does apply to dynamical systems that are not autonomous, i.e., that may be subject to time-dependent forcing. The latter is certainly the case for the climate system on time scales of 10–100 Kyr and longer, which is affected strongly by orbital forcing.

Ref. (*89*) distinguished between large-scale *typology* and small-scale *texture* in the interpretation of square matrix of dots that is the visual result of RP. Thus, if all the characteristic times of an autonomous dynamical system are short compared to the length of the time series, the RP's typology will be homogeneous and, thus, not very interesting. In the presence of an imposed drift, a more interesting typology will appear. The most interesting typology in RP applications so far is associated with recurrent patterns that are not exactly periodic but only nearly so. Hence, such patterns are not that easily detectable by purely spectral approaches to time series analysis. Ref. (*90*) discussed how to render the purely visual RP typologies studied up to that point more objectively quantifiable by recurrence quantification analysis and bootstrapping (*91*, *92*). The RP exhibits, moreover, a characteristic texture — given by the pattern of vertical and horizontal lines that mark recurrences. These lines sometimes form recurrence clusters that correspond to specific periodic patterns.

Quasi-potential, Melancholia States, and Critical Transitions

Traditionally, tipping points are schematically represented as being associated with the bifurcation occurring for a system described by a one-dimensional effective potential when a change in the value of a certain parameter leads to a change in the number of stable equilibriums. Hence, conditions describing the nearing of a tipping point can be related to the presence of slower decay of correlations (critical slowing down). This viewpoint, while attractive, suffers from many mathematical issues due to the fact that the true dynamics of the system occurs in a possibly very high dimensional space. Refs. (*93*, *94*) have introduced a mathematically rigorous framework for the occurrence of tipping points that clarifies the link between rate of decay of correlations, sensitivity of the system to perturbations, and robustness of the unperturbed dynamics.

Here we wish to take a different angle on the problem, where, instead, of focusing on the approach to the individual tipping points, we try to capture the global stability properties of the system, Indeed, taking inspiration from the use of the Waddington epigenetic landscape to describe evolution (*39–43*) and from the theory of punctuated equilibrium (*44*, *45*), Refs. (*36*, *37*) proposed to describe the global properties of the climate system using the formalism of quasi-potential (*38*). Roughly speaking, assuming that the system lives in $\mathbb{R}^N$, and its dynamics is described by a stochastic differential equation the probability that its state is within the volume $d\vec{x}$ around the point $\vec{x} \in \mathbb{R}^N$ is given by $P(\vec{x}, d\vec{x}) = \rho(\vec{x})d\vec{x}$ where $\rho(\vec{x}) \approx e^{-\frac{2\Phi(\vec{x})}{\varepsilon^2}}$ is the probability distribution function (pdf) and $\Phi(\vec{x})$ is the quasipotential. The function $\Phi(\vec{x})$ depends in a nontrivial way on the drift term and noise law defining the stochastic differential equation. This setting generalizes the classical energy landscape and applies to a fairly large class of stochastic dynamical systems. One can see the dynamics of the system as being driven towards lower values $\Phi(\vec{x})$ (plus an extra rotational effect that is typical of non-equilibrium systems), while the stochastic forcing noise makes sure that the system is erratically pushed around. Hence, the minima of $\Phi(\vec{x})$ correspond to local maxima of the pdf, and the saddles (which coincide for both $\Phi(\vec{x})$ and $\rho(\vec{x})$) correspond to the Melancholia (M) states (*31*). Such M states are unstable states of the system that live at the boundary between basins of attraction and are the gateways for the noise-induced transitions between competing stable states. Ref. (*34*) applied this angle to the investigation of the metastability properties of an intermediate complexity climate model and suggested that the presence of decorations of the quasi-potential at different scales could be interpreted as being associated with a hierarchy of tipping points. Indeed, passing near M states is intimately associated with the occurrence of critical transitions. Hence, the construction of the quasi-potential $\Phi(\vec{x})$ can be seen as the structural counterpart of the investigation of the time-evolution of the system and of its critical transitions. Ref. (*95*) gives a complete overview of different methods applied to perform such analysis.

REFERENCES

1. W. Dansgaard, S. J. Johnsen, J. Moller, C. C. Langway, One thousand centuries of climatic record from Camp Century on the Greenland ice sheet. *Science*. **166**, 377–381 (1969).
2. W. Dansgaard, H. B. Clausen, N. Gundestrup, C. U. J. Hammer, S. F. ohnsen, P. M. Kristinsdottir, N. Reeh, A new Greenland deep ice core. *Science*. **218**, 1273–1277 (1982).
3. W. Broecker, Climatic Change - Are we on the brink of a pronounced global warming. *Science*. **189**, 460–463 (1975).
4. W. S. Broecker, M. Andree, G. Bonani, W. Wolfi, H. Oeschger, M. Klas, Can the Greenland climatic jumps be identified in records from ocean and land? *Quat. Res.* **30**, 1–6 (1988).
5. W. S. Broecker, G. Denton, The role of ocean-atmosphere reorganizations in glacial cycles. *Geochim Cosmochim Acta*. **53**, 2465–2501 (1989).
6. S. O. Rasmussen, M. Bigler, S. P. Blockley, T. Blunier, S. L. Buchardt, H. B. Clausen, I. Cvijanovic, D. Dahl-Jensen, S. J. Johnsen, H. Fischer, V. Gkinis, M. Guillevic, W. Z. Hoek, J. J. Lowe, J. B. Pedro, T. Popp, I. K. Seierstad, J. P. Steffensen, A. M. Svensson, P. Vallelonga, B. M. Vinther, M. J. C. Walker, J. J. Wheatley, M. Winstrup, A stratigraphic framework for abrupt climatic changes during the Last Glacial period based on three synchronized Greenland ice-core records: refining and extending the INTIMATE event stratigraphy. *Quat. Sci. Rev.* **106**, 14–28 (2014).
7. P. F. Hoffman, D. S. Abbot, Y. Ashkenazy, D. I. Benn, J. J. Brocks, P. A. Cohen, G. M. Cox, J. R. Creveling, Y. Donnadieu, D. H. Erwin, I. J. Fairchild, D. Ferreira, J. C. Goodman, G. P. Halverson, M. F. Jansen, G. Le Hir, G. D. Love, F. A. Macdonald, A. C. Maloof, C. A. Partin, G. Ramstein, B. E. J. Rose, C. V. Rose, P. M. Sadler, E. Tziperman, A. Voigt, S. G. Warren, Snowball Earth climate dynamics and Cryogenian geology-geobiology. *Sci. Adv.* **3** (2017), doi:10.1126/sciadv.1600983.
8. C. R. Scotese, H. Song, B. J. W. Mills, D. G. van der Meer, Phanerozoic paleotemperatures: The earth's changing climate during the last 540 million years. *Earth-Sci. Rev.* **215** (2021), doi:10.1016/j.earscirev.2021.103503.
9. M. Grodzins, Metropolitan segregation. *Sci. Am.* **197**, 33- (1957).
10. M. Gladwell, *The Tipping Point: How Little Things Can Make a Big Difference* (Back Bay Books, Bosto,, New York, London, 2002).
11. T. Lenton, H. Held, E. Kriegler, J. Hall, W. Lucht, S. Rahmstorf, H. Schellnhuber, Tipping elements in the Earth's climate system. *Proc. Natl. Acad. Sci. U. S. A.* **105**, 1786–1793 (2008).
12. T. Lenton, "Environmental Tipping Points" in *Annual review of Environment and Resources*, A. Gadgil, D. Liverman, Eds. (2013), vol. 38, pp. 1–29.
13. T. Lenton, J. Rockstrom, O. Gaffney, S. Rahmstorf, K. Richardson, W. Steffen, H. Schellnhuber, Climate tipping points - too risky to bet against. *Nature*. **575**, 592–595 (2019).

14. V. Brovkin, E. Brook, J. Williams, S. Bathiany, T. Lenton, M. Barton, R. DeConto, J. Donges, A. Ganopolski, J. McManus, S. Praetorius, A. de Vernal, A. Abe-Ouchi, H. Cheng, M. Claussen, M. Crucifix, G. Gallopin, V. Iglesias, D. Kaufman, T. Kleinen, F. Lambert, S. van der Leeuw, H. Liddy, M. Loutre, D. McGee, K. Rehfeld, R. Rhodes, A. Seddon, M. Trauth, L. Vanderveken, Z. Yu, Past abrupt changes, tipping points and cascading impacts in the Earth system. *Nat. Geosci.* **14**, 550–558 (2021).

15. T. Lenton, H. Williams, On the origin of planetary-scale tipping points. *Trends Ecol. Evol.* **28**, 380–382 (2013).

16. W. Steffen, J. Rockstrom, K. Richardson, T. Lenton, C. Folke, D. Liverman, C. Summerhayes, A. Barnosky, S. Cornell, M. Crucifix, J. Donges, I. Fetzer, S. Lade, M. Scheffer, R. Winkelmann, H. Schellnhuber, Trajectories of the Earth System in the Anthropocene. *Proc. Natl. Acad. Sci. U. S. A.* **115**, 8252–8259 (2018).

17. E. Kriegler, J. Hall, H. Held, R. Dawson, H. Schellnhuber, Imprecise probability assessment of tipping points in the climate system. *Proc. Natl. Acad. Sci. U. S. A.* **106**, 5041–5046 (2009).

18. N. Wunderling, J. Donges, J. Kurths, R. Winkelmann, Interacting tipping elements increase risk of climate domino effects under global warming. *Earth Syst. Dyn.* **12**, 601–619 (2021).

19. N. Boers, Observation-based early-warning signals for a collapse of the Atlantic Meridional Overturning Circulation (vol 11, pg 680, 2021). *Nat. Clim. Change*. **11**, 1001–1001 (2021).

20. I. Otto, J. Donges, R. Cremades, A. Bhowmik, R. Hewitte, W. Lucht, J. Rockstrom, F. Allerberger, M. McCaffrey, S. Doe, A. Lenferna, N. Moran, D. van Vuuren, H. Schellnhuber, Social tipping dynamics for stabilizing Earth's climate by 2050. *Proc. Natl. Acad. Sci. U. S. A.* **117**, 2354–2365 (2020).

21. T. Lenton, S. Benson, T. Smith, T. Ewer, V. Lanel, E. Petykowski, T. Powell, J. Abrams, F. Blomsma, S. Sharpe, Operationalising positive tipping points towards global sustainability. *Glob. Sustain.* **5** (2022), doi:10.1017/sus.2021.30.

22. T. Westerhold, N. Marwan, A. J. Drury, D. Liebrand, C. Agnini, E. Anagnostou, J. S. K. Barnet, S. M. Bohaty, D. De Vleeschouwer, F. Florindo, T. Frederichs, D. A. Hodell, A. E. Holbourn, D. Kroon, V. Lauretano, K. Littler, L. J. Lourens, M. Lyle, H. Palike, U. Rohl, J. Tian, R. H. Wilkens, P. A. Wilson, J. C. Zachos, An astronomically dated record of Earth's climate and its predictability over the last 66 million years. *Science*. **369**, 1383-+ (2020).

23. D. A. Hodell, J. E. T. Channell, Mode transitions in Northern Hemisphere glaciation: co-evolution of millennial and orbital variability in Quaternary climate. *Clim. Past*. **12**, 1805–1828 (2016).

24. W. Bagniewski, M. Ghil, D. D. Rousseau, Automatic detection of abrupt transitions in paleoclimate records. *Chaos*. **31** (2021), doi:10.1063/5.0062543.

25. H. Stommel, Thermohaline convection with 2 stable regimes of flow. *Tellus*. **13**, 224–230 (1961).

26. W. D. Sellers, A Global Climatic Model Based on the Energy Balance of the Earth-Atmosphere System. *J. Appl. Meteorol. Climatol.* **8**, 392–400 (1969).

27. M. Budyko, Effect of solar radiation variations on climate of earth. *Tellus*. **21**, 611- (1969).

28. M. Ghil, Climate stability for a Sellers-type model. *J. Atmospheric Sci.* **33**, 3–20 (1976).

29. M. Ghil, A Century of Nonlinearity in the Geosciences. *Earth Space Sci.* **6**, 1007–1042 (2019).

30. M. Ghil, V. Lucarini, The physics of climate variability and climate change. *Rev. Mod. Phys.* **92** (2020), doi:10.1103/RevModPhys.92.035002.

31. V. Lucarini, T. Bodai, Edge states in the climate system: exploring global instabilities and critical transitions. *Nonlinearity*. **30**, R32–R66 (2017).

32. J. Lewis, A. Weaver, M. Eby, Snowball versus slushball Earth: Dynamic versus nondynamic sea ice? *J. Geophys. Res.-Oceans*. **112** (2007), doi:10.1029/2006JC004037.

33. D. Abbot, A. Voigt, D. Koll, The Jormungand global climate state and implications for Neoproterozoic glaciations. *J. Geophys. Res.-Atmospheres*. **116** (2011), doi:10.1029/2011JD015927.
34. G. Margazoglou, T. Grafke, A. Laio, V. Lucarini, Dynamical landscape and multistability of a climate model. *Proc. R. Soc. -Math. Phys. Eng. Sci.* **477** (2021), doi:10.1098/rspa.2021.0019.
35. C. Ragon, V. Lembo, V. Lucarini, C. Verard, J. Kasparian, M. Brunetti, Robustness of Competing Climatic States. *J. Clim.* **35**, 2769–2784 (2022).
36. V. Lucarini, T. Bodai, Transitions across Melancholia States in a Climate Model: Reconciling the Deterministic and Stochastic Points of View. *Phys. Rev. Lett.* **122** (2019), doi:10.1103/PhysRevLett.122.158701.
37. V. Lucarini, T. Bodai, Global stability properties of the climate: Melancholia states, invariant measures, and phase transitions. *Nonlinearity*. **33**, R59–R92 (2020).
38. R. Graham, "Macroscopic potentials, bifurcations and noise in dissipative systems" in *Fluctuations and stochastic phenomena in condensed matter* (Springer, 1987), pp. 1–34.
39. C. H. Waddington, Canalization of development and the inheritance of acquired characters. *Nature*. **150**, 563–565 (1942).
40. C. H. Waddington, *The strategy of the genes* (Allen & Unwin, London, 1957).
41. A. D. Goldberg, C. D. Allis, E. Bernstein, Epigenetics: a landscape takes shape. *Cell*. **128**, 635–638 (2007).
42. J. Baedke, The epigenetic landscape in the course of time: Conrad Hal Waddington’s methodological impact on the life sciences. *Stud. Hist. Philos. Sci. Part C Stud. Hist. Philos. Biol. Biomed. Sci.* **44**, 756–773 (2013).
43. M. Allen, Compelled by the diagram: thinking through CH Waddington’s epigenetic landscape. *Contemporaneity*. **4**, 119 (2015).
44. N. Eldredge, S. J. Gould, "Punctuated Equilibria: An alternative to Phyletic Gradualism" in *Models in Paleobiology*, T. J. M. Schopf, Ed. (Freeman Cooper, San Francisco, 1972), pp. 82–243.
45. S. J. Gould, N. Eldredge, Punctuated equilibria : the tempo and mode of evolution reconsidered. *Paleobiology*. **3**, 115–151 (1977).
46. K. Christensen, S. de Collobiano, M. Hall, H. Jensen, Tangled nature: A model of evolutionary ecology. *J. Theor. Biol.* **216**, 73–84 (2002).
47. H. J. Jensen, Tangled Nature: A model of emergent structure and temporal mode among co-evolving agents. *Eur. J. Phys.* **40** (2019), doi:10.1088/1361-6404/aaee8f.
48. J. Zachos, M. Pagani, L. Sloan, E. Thomas, K. Billups, Trends, rhythms, and aberrations in global climate 65 Ma to present. *Science*. **292**, 686–693 (2001).
49. N. Marwan, M. Carmen Romano, M. Thiel, J. Kurths, Recurrence plots for the analysis of complex systems. *Phys. Rep.* **438**, 237–329 (2007).
50. J. Zachos, J. Breza, S. Wise, Early Oligocene ice-sheet expansion on Antractica - stable isotope and sedimentological evidence from Kerguelen Plateau, Southern Indian-Ocean. *Geology*. **20**, 569–573 (1992).
51. L. Ivany, W. Patterson, K. Lohmann, Cooler winters as a possible cause of mass extinctions at the eocene/oligocene boundary. *Nature*. **407**, 887–890 (2000).
52. J. Sun, X. Ni, S. Bi, W. Wu, J. Ye, J. Meng, B. Windley, Synchronous turnover of flora, fauna, and climate at the Eocene-Oligocene Boundary in Asia. *Sci. Rep.* **4** (2014), doi:10.1038/srep07463.
53. E. Thomas, J. C. Zachos, T. J. Bralower, "Deep-sea environments on a warm earth: latest Paleocene-early Eocene" in *Warm Climates in Earth History*, B. T. Huber, K. G. Macleod, S. L. Wing, Eds. (Cambridge University Press, Cambridge, 1999; https://www.cambridge.org/core/books/warm-climates-in-earth-history/deepsea-environments-on-a-warm-earth-latest-paleoceneearly-eocene/5812213E2DDEB85D28B654244C4ECE86), pp. 132–160.
54. K. Miller, J. Browning, W. Schmelz, R. Kopp, G. Mountain, J. Wright, Cenozoic sea-level and cryospheric evolution from deep-sea geochemical and continental margin

records. *Sci. Adv.* **6** (2020), doi:10.1126/sciadv.aaz1346.
55. J. Kennett, L. Stott, Abrupt deep-sea warming, palaeoceanographic changes and benthic extinctions at the end of the Paleocene. *Nature*. **353**, 225–229 (1991).
56. G. R. Dickens, M. M. Castillo, J. C. Walker, A blast of gas in the latest Paleocene: simulating first-order effects of massive dissociation of oceanic methane hydrate. *Geology*. **25 3**, 259–62 (1997).
57. V. Lauretano, A. Kennedy-Asser, V. Korasidis, M. Wallace, P. Valdes, D. Lunt, R. Pancost, B. Naafs, Eocene to Oligocene terrestrial Southern Hemisphere cooling caused by declining pCO(2). *Nat. Geosci.* **14**, 659-+ (2021).
58. J. Kennett, N. Shackleton, Oxugen isotopic evidence for development of psychrosphere 38 Myr ago. *Nature*. **260**, 513–515 (1976).
59. N. J. Shackleton, "Oceanic Carbon Isotope Constraints on Oxygen and Carbon Dioxide in the Cenozoic Atmosphere" in *The Carbon Cycle and Atmospheric CO2: Natural Variations Archean to Present* (American Geophysical Union (AGU), 1985; https://agupubs.onlinelibrary.wiley.com/doi/abs/10.1029/GM032p0412), pp. 412–417.
60. H. Palike, M. Lyle, H. Nishi, I. Raffi, A. Ridgwell, K. Gamage, A. Klaus, G. Acton, L. Anderson, J. Backman, J. Baldauf, C. Beltran, S. Bohaty, P. Bown, W. Busch, J. Channell, C. Chun, M. Delaney, P. Dewangan, T. Dunkley Jones, K. Edgar, H. Evans, P. Fitch, G. Foster, N. Gussone, H. Hasegawa, E. Hathorne, H. Hayashi, J. Herrle, A. Holbourn, S. Hovan, K. Hyeong, K. Iijima, T. Ito, S. Kamikuri, K. Kimoto, J. Kuroda, L. Leon-Rodriguez, A. Malinverno, T. Moore, B. Murphy, D. Murphy, H. Nakamura, K. Ogane, C. Ohneiser, C. Richter, R. Robinson, E. Rohling, O. Romero, K. Sawada, H. Scher, L. Schneider, A. Sluijs, H. Takata, J. Tian, A. Tsujimoto, B. Wade, T. Westerhold, R. Wilkens, T. Williams, P. Wilson, Y. Yamamoto, S. Yamamoto, T. Yamazaki, R. Zeebe, A Cenozoic record of the equatorial Pacific carbonate compensation depth. *Nature*. **488**, 609-+ (2012).
61. D. Beerling, D. Royer, Convergent Cenozoic CO2 history. *Nat. Geosci.* **4**, 418–420 (2011).
62. R. DeConto, D. Pollard, P. Wilson, H. Palike, C. Lear, M. Pagani, Thresholds for Cenozoic bipolar glaciation. *Nature*. **455**, 652-U52 (2008).
63. IPCC, *Climate Change 2021: The Physical Science Basis. Contribution of Working Group I to the Sixth Assessment Report of the Intergovernmental Panel on Climate Change* (Cambridge University Press, Cambridge, United Kingdom and New York, NY, USA, 2021), vol. In Press.
64. J. D. O'Keefe, T. J. Ahrens, Impact production of C02 by the Cretaceous/Tertiary extinction bolide and the resultant heating of the Earth. *Nature*. **338**, 247–249 (1989).
65. B. Lomax, D. Beerling, G. Upchurch, B. Otto-Bliesner, Rapid (10-yr) recovery of terrestrial productivity in a simulation study of the terminal Cretaceous impact event. *Earth Planet. Sci. Lett.* **192**, 137–144 (2001).
66. D. W. Jolley, B. R. Bell, "The North Atlantic Igneous Province: Stratigraphy, Tectonic, Volcanic, and Magmatic Processes" in (Geological Society of London, 2002).
67. K. Birkenmajer, A. Gaździcki, K. P. Krajewski, A. Przybycin, A. Solecki, A. Tatur, H. I. Yoon, First Cenozoic glaciers in west Antarctica. *Pol. Polar Res.*, 3-12-3–12 (2005).
68. K. Rose, F. Ferraccioli, S. Jamieson, R. Bell, H. Corr, T. Creyts, D. Braaten, T. Jordan, P. Fretwell, D. Damaske, Early East Antarctic Ice Sheet growth recorded in the landscape of the Gamburtsev Subglacial Mountains. *Earth Planet. Sci. Lett.* **375**, 1–12 (2013).
69. C. Janis, Tertiary mammal evolution in the context of changing climates, vegetation, and tectonic events. *Annu. Rev. Ecol. Syst.* **24**, 467–500 (1993).
70. T. H. Torsvik, L. R. M. Cocks, *Earth history and palaeogeography* (Cambridge University Press, 2016).
71. Y. Lagabrielle, Y. Godderis, Y. Donnadieu, J. Malavieille, M. Suarez, The tectonic history of Drake Passage and its possible impacts on global climate. *Earth Planet. Sci. Lett.* **279**, 197–211 (2009).

72. D. Rowley, B. Currie, Palaeo-altimetry of the late Eocene to Miocene Lunpola basin, central Tibet. *Nature*. **439**, 677–681 (2006).
73. O. Bialik, M. Frank, C. Betzler, R. Zammit, N. Waldmann, Two-step closure of the Miocene Indian Ocean Gateway to the Mediterranean. *Sci. Rep.* **9** (2019), doi:10.1038/s41598-019-45308-7.
74. D. Lunt, P. Valdes, A. Haywood, I. Rutt, Closure of the Panama Seaway during the Pliocene: implications for climate and Northern Hemisphere glaciation. *Clim. Dyn.* **30**, 1–18 (2008).
75. J. Chappell, N. J. Shackleton, Oxygen isotopes and sea-level. *Nature*. **324**, 137–140 (1986).
76. N. J. Shackleton, The 100,000-year ice-age cycle identified and found to lag temperature, carbon dioxide, and orbital eccentricity. *Science*. **289**, 1897–1902 (2000).
77. H. Elderfield, P. Ferretti, M. Greaves, S. Crowhurst, I. N. McCave, D. Hodell, A. M. Piotrowski, Evolution of Ocean Temperature and Ice Volume Through the Mid-Pleistocene Climate Transition. *Science*. **337**, 704–709 (2012).
78. S. K. Turner, Pliocene switch in orbital-scale carbon cycle/climate dynamics. *Paleoceanography*. **29**, 1256–1266 (2014).
79. D. Rousseau, W. Bagniewski, M. Ghil, Abrupt climate changes and the astronomical theory: are they related? *Clim. Past*. **18**, 249–271 (2022).
80. N. J. Shackleton, N. D. Opdyke, Oxygen isotope and palaeomagnetic evidence for early Northern Hemisphere glaciation. *Nature*. **270**, 216–223 (1977).
81. N. G. Pisias, T. C. Moore, The evolution of Pleistocene climate: A time-series approach. *Earth Planet. Sci. Lett.* **52**, 450–458 (1981).
82. W. F. Ruddiman, M. Raymo, D. G. Martinson, B. M. Clement, J. Backman, Pleistocene evolution : Northern Hemisphere ice sheets and North Atlantic Ocean. *Paleoceanography,*. **4**, 353–412 (1989).
83. P. U. Clark, D. Pollard, Origin of the middle Pleistocene transition by ice sheet erosion of regolith. *Paleoceanography*. **13**, 1–9 (1998).
84. P. U. Clark, D. Archer, D. Pollard, J. D. Blum, J. A. Rial, V. Brovkin, A. C. Mix, N. G. Pisias, M. Roy, The middle Pleistocene transition: characteristics. mechanisms, and implications for long-term changes in atmospheric PCO2. *Quat. Sci. Rev.* **25**, 3150–3184 (2006).
85. C. Boettner, G. Klinghammer, N. Boers, T. Westerhold, N. Marwan, Early-warning signals for Cenozoic climate transitions. *Quat. Sci. Rev.* **270** (2021), doi:10.1016/j.quascirev.2021.107177.
86. D. Pollard, R. DeConto, Continuous simulations over the last 40 million years with a coupled Antarctic ice sheet-sediment model. *Palaeoclimatol. Palaeoecol. Palaeogeogr.* **537** (2020), doi:10.1016/j.palaeo.2019.109374.
87. C. L. Batchelor, M. Margold, M. Krapp, D. Murton, A. S. Dalton, P. L. Gibbard, C. R. Stokes, J. B. Murton, A. Manica, The configuration of Northern Hemisphere ice sheets through the Quaternary. *Nat. Commun.* **10** (2019), doi:10.1038/s41467-019-11601-2.
88. W. Bagniewski, D.-D. Rousseau, Ghil, Michael, PaleoJump: A database for abrupt transitions in past climates. *arXiv* (2022), p. doi:10.48550/arxiv.2206.06832D.
89. J. P. Eckmann, S. O. Kamphorst, D. Ruelle, Recurrence plots of dynamical systems. *Europhys. Lett.* **4**, 973–977 (1987).
90. N. Marwan, S. Schinkel, J. Kurths, Recurrence plots 25 years later - Gaining confidence in dynamical transitions. *EPL*. **101** (2013), doi:10.1209/0295-5075/101/20007.
91. B. Efron, nonparametric estimates of standard error - The Jackknife, the bootstrap and other methods. *Biometrika*. **68**, 589–599 (1981).
92. B. Efron, R. Tibshirani, Bootstrap methods for standard errors, confidence intervals, and other measures of statistical accuracy. *Stat. Sci.* **1**, 54–75 (1986).
93. A. Tantet, V. Lucarini, H. Dijkstra, Resonances in a Chaotic Attractor Crisis of the Lorenz Flow. *J. Stat. Phys.* **170**, 584–616 (2018).
94. A. Tantet, V. Lucarini, F. Lunkeit, H. Dijkstra, Crisis of the chaotic attractor of a climate

model: a transfer operator approach. *Nonlinearity*. **31**, 2221–2251 (2018).
95. J. X. Zhou, M. D. S. Aliyu, E. Aurell, S. Huang, Quasi-potential landscape in complex multi-stable systems. *J. R. Soc. Interface*. **9**, 3539–3553 (2012).
96. K. Miller, J. Wright, R. Fairbanks, Unlocking the ice-house Oligocene-Miocene oxygen isotopes, eustasy, and margin erosion. *J. Geophys. Res.-Solid Earth Planets*. **96**, 6829–6848 (1991).
97. S. Boulila, B. Galbrun, K. Miller, S. Pekar, J. Browning, J. Laskar, J. Wright, On the origin of Cenozoic and Mesozoic “third-order” eustatic sequences. *Earth-Sci. Rev.* **109**, 94–112 (2011).
98. G. Paxman, S. Jamieson, K. Hochmuth, K. Gohl, M. Bentley, G. Leitchenkov, F. Ferraccioli, Reconstructions of Antarctic topography since the Eocene-Oligocene boundary. *Palaeoclimatol. Palaeoecol. Palaeogeogr.* **535** (2019), doi:10.1016/j.palaeo.2019.109346.
99. E. Rohling, J. Yu, D. Heslop, G. Foster, B. Opdyke, A. Roberts, Sea level and deep-sea temperature reconstructions suggest quasi-stable states and critical transitions over the past 40 million years. *Sci. Adv.* **7** (2021), doi:10.1126/sciadv.abf5326.
100. A. Houben, C. van Mourik, A. Montanari, R. Coccioni, H. Brinkhuis, The Eocene-Oligocene transition: Changes in sea level, temperature or both? *Palaeoclimatol. Palaeoecol. Palaeogeogr.* **335**, 75–83 (2012).
101. Y. Smith, D. Hill, A. Dolan, A. Haywood, H. Dowsett, B. Risebrobakken, Icebergs in the Nordic Seas Throughout the Late Pliocene. *Paleoceanogr. Paleoclimatology*. **33**, 318–335 (2018).
102. I. Bailey, G. Hole, G. Foster, P. Wilson, C. Storey, C. Trueman, M. Raymo, An alternative suggestion for the Pliocene onset of major northern hemisphere glaciation based on the geochemical provenance of North Atlantic Ocean ice-rafted debris. *Quat. Sci. Rev.* **75**, 181–194 (2013).
103. B. D. A. Naafs, J. Hefter, R. Stein, Millennial-scale ice rafting events and Hudson Strait Heinrich(-like) Events during the late Pliocene and Pleistocene: a review. *Quat. Sci. Rev.* **80**, 1–28 (2013).
104. R. S. W. van de Wal, B. de Boer, L. J. Lourens, P. Koehler, R. Bintanja, Reconstruction of a continuous high-resolution CO2 record over the past 20 million years. *Clim. Past*. **7**, 1459–1469 (2011).
105. K. A. Jakob, P. A. Wilson, J. Pross, T. H. G. Ezard, J. Fiebig, J. Repschlager, O. Friedrich, A new sea-level record for the Neogene/Quaternary boundary reveals transition to a more stable East Antarctic Ice Sheet. *Proc. Natl. Acad. Sci. U. S. A.* **117**, 30980–30987 (2020).
106. G. Muttoni, C. Carcano, E. Garzanti, M. Ghielmi, A. Piccin, R. Pini, S. Rogledi, D. Sciunnach, Onset of major Pleistocene glaciations in the Alps. *Geology*. **31**, 989–992 (2003).
107. M. F. Knudsen, J. Norgaard, R. Grischott, F. Kober, D. L. Egholm, T. M. Hansen, J. D. Jansen, New cosmogenic nuclide burial-dating model indicates onset of major glaciations in the Alps during Middle Pleistocene Transition. *Earth Planet. Sci. Lett.* **549** (2020), doi:10.1016/j.epsl.2020.116491.
108. C. J. Berends, B. de Boer, R. S. W. van de Wal, Reconstructing the evolution of ice sheets, sea level, and atmospheric CO2 during the past 3.6 million years. *Clim. Past*. **17**, 361–377 (2021).
109. O. Seki, G. L. Foster, D. N. Schmidt, A. Mackensen, K. Kawamura, R. D. Pancost, Alkenone and boron-based Pliocene pCO(2) records. *Earth Planet. Sci. Lett.* **292**, 201–211 (2010).
110. W. S. Broecker, J. van Donk, Insolation changes, ice volumes, and 0-18 record in deep-sea cores. *Rev. Geophys. Space Phys.* **8**, 169–198 (1970).
111. S. Barker, G. Knorr, R. L. Edwards, F. Parrenin, A. E. Putnam, L. C. Skinner, E. Wolff, M. Ziegler, 800,000 Years of Abrupt Climate Variability. *Science*. **334**, 347–351 (2011).
112. J. F. McManus, D. W. Oppo, J. L. Cullen, A 0,5-million-year record of millennial-scale

climate variability in the North Atlantic. *Science*. **283**, 971–975 (1999).

113. H. Heinrich, Origin and Consequences of Cyclic Ice Rafting in the Northeast Atlantic Ocean during the Past 130,000 years. *Quat. Res.* **29**, 142–152 (1988).
114. G. Bond, H. Heinrich, W. Broecker, L. Labeyrie, J. McManus, J. Andrews, S. Huon, R. Jantschik, S. Clasen, C. Simet, K. Tedesco, M. Klas, G. Bonani, S. Ivy, Evidence for massive discharges of icebergs into the North Atlantic Ocean during the last glacial period. *Nature*. **360**, 245–249 (1992).
115. G. Bond, W. Broecker, S. Johnsen, J. McManus, L. Labeyrie, J. Jouzel, G. Bonani, Correlations between climate records from North Atlantic sediments and Greenland ice. *Nature*. **365**, 143–147 (1993).
116. S. P. Obrochta, T. J. Crowley, J. E. T. Channell, D. A. Hodell, P. A. Baker, A. Seki, Y. Yokoyama, Climate variability and ice-sheet dynamics during the last three glaciations. *Earth Planet. Sci. Lett.* **406**, 198–212 (2014).
117. J. Jouzel, V. Masson-Delmotte, O. Cattani, G. Dreyfus, S. Falourd, G. Hoffmann, B. Minster, J. Nouet, J. Barnola, J. Chappellaz, H. Fischer, J. Gallet, S. Johnsen, M. Leuenberger, L. Loulergue, D. Luethi, H. Oerter, F. Parrenin, G. Raisbeck, D. Raynaud, A. Schilt, J. Schwander, E. Selmo, R. Souchez, R. Spahni, B. Stauffer, J. Steffensen, B. Stenni, T. Stocker, J. Tison, M. Werner, E. Wolff, Orbital and millennial Antarctic climate variability over the past 800,000 years. *Science*. **317**, 793–796 (2007).

Acknowledgments

We would like to thank our colleagues from Horizon 2020 TiPES project (grant No. 820970) and especially Michael Ghil for useful discussions about this study. This is LDEO contribution and TiPES contribution XXX. VL acknowledges useful exchanges with T. Bodai, R. Boerner, R. Deeley, G. Margazoglou, C. Nesbitt, and L. Serdukova.

Funding:

This research has been supported by the European Commission, Horizon 2020 Framework Programme (TiPES, grant no. 820970), by the Marie Cure ITN Critical Earth (Grant No. 956170) and from the EPSRC Project No. EP/T018178/1

Author contributions: Conceptualization: DDR; Methodology, investigation and Visualization: DDR, VL, WB; Writing—original draft: DDR; Writing—review & editing: DDR, VL, WB

Competing interests: All authors declare they have no competing interests.

Data and materials availability: All data generated by the present study from the main text or the supplementary materials will be submitted to PANGAEA data repository. U1308 marine data are available at https://doi.org/10.1594/PANGAEA.871937 (Hodell and Channell, 2016b). CENOGRID data are available at https://doi.org/10.1594/PANGAEA.917503 (Westerhold, 2020).

Figures and Tables

Fig. 1. **KS test and Recurrence Quantitative Analysis (RQA) of CENOGRID benthic δ^{18}O.** A) Time series in Ma BP with difference of the reconstructed and present Mean Global Temperature in pink). KS test identifying abrupt transitions towards warmer conditions in red and cooler or colder conditions in blue; B) Recurrence plot (RP) with identification of the main two clusters prior and after 34 Ma. The main abrupt transitions identified are highlighted by red circles, and C) Recurrence rate (RR). The pink crosses and vertical green lines indicate the abrupt transitions (TP) detected by the RQA. CENOGRID benthic δ^{18}O data are from (*22*)

Fig. 2. **Variation through time of three main climate factors and comparison with the identified abrupt transitions (TP) in the CENOGRID benthic δ^{18}O.** A) Global Mean Sea Level in meters from (*54*). Identification of particular warm and of glaciation events. The Laurentide, GIW-WAIS and Ice free lines are from (*54*); B) Carbonate Compensation Depth (CCD) in meters from (*60*). The purple circles identify the TPs on this record; C) Estimate of the CO_2 concentration in parts per million volume (ppmv) from (*61*). The Antarctica glaciation threshold at 750 ppmv and the NH glaciation threshold at 280 ppmv lines respectively are from (*62*).

Fig. 3. **Probability density of the climate system in the projected CENOGRID benthic δ^{18}O and δ^{13}C. space.** Panel a) Chronologically ordered TP_Os (diamonds) selected according to the KS methodology for δ^{18}O with time window 1-4 My are shown. The two extra TP_Os found via RP are indicated with a *. Panel b) Chronologically ordered fast TP_Os (FTP_Os, diamonds) selected according to the KS methodology for δ^{18}O with time window 0.25-1 Myr are shown. Panel c) Same as a), but for the δ^{13}C record. The approximate timing of the TPs is indicated (rounded to .01 My). The 5 Ky-long portions of trajectories before and after each TP are also plotted.

Fig. 4. **RQA of U1308 benthic δ^{18}O**. A) Time series in Ma; B) RP; and C) RR. Crosses similar than Fig. S1. TPo9-10 and RTPo1-4 abrupt transitions identified in the RR. U1308 benthic δ^{18}O data are from (*23*)

Fig. 5. **Evolution of the Earth Climate history among 2 different tipping landscapes and proposal for a potential third one.** The first landscape in light red, corresponds to the Hot-Warm House time interval. The second landscape in light blue corresponds to the Cold-Ice house time interval. The third landscape, in light green, corresponds to the potential new one represented

by the Anthropocene time interval. The different abrupt transitions identified in the present study are reported as TPo or RTPo to differentiate the major tipping points from the critical transitions characterizing transitions of lighter significance in the climate history. Various plate tectonic and ice sheet events are indicated and supported by maps of plate movements and North and South Hemisphere ice sheets. The Antarctica maps are from (*86*), Northern Hemisphere ice sheet maps are from (*87*). The paleogeographic maps have been generated using the Ocean Drilling Stratigraphic Network (ODSN) plate tectonic reconstruction service: <https://www.odsn.de/odsn/services/paleomap/paleomap.html>. The red arrows on the tectonic maps indicate the key events at the identified abrupt transition.

SUPPLEMENTARY MATERIALS

Please use the *Science Advances* template to format your Supplementary Materials.

Supplementary Text

Comparison between GMSL, CCD and CO_2 concentration from CENOGRID (past 66 Myr)

The interval between 66 Ma and 63 Ma (TP_o1) shows a relative stable GMSL above +60m. It is followed by a lowering corresponding to a decreasing trend of about 70m in several steps between TP_o1 at 63 Ma and TP_o3 at 56 Ma, punctuated by an abrupt increase of 52m, at TP_o2 around 58 Ma, and another of 28m corresponding to the short but intense Paleocene-Eocene Thermal Maximum (PETM – Fig. 3a) warming. GMSL raises between TP_o2 at 58 Ma and 55 Ma by about +40m. The interval between 55 Ma and 48 Ma, the Early Eocene climatic optimum (EEOC – Fig. 2A), indicates a relatively high GMSL of about 66 m above the present mean sea level, which is associated with the occurrence of hyperthermal conditions at 58 Ma, 57 Ma, 53 Ma. Between 52 Ma and TP4 at about 47 Ma, CCD reaches the shallowest depth of the record, about 3000m, (*60*) associated with the highest CO2 concentrations estimated above 1100 ppmv by Ref (*61*) – Fig. 2B,C). A strong decrease in GMSL of about 30m occurs between 48 Ma and 46 Ma while it remains relatively stable at about +42m between 46 Ma and TP5, at 40 Ma. It is however punctuated by two short events, first a lowering of about 25m between 42 Ma and 40.5 Ma, and strong increase of about 40m between 40.5 Ma and 40 Ma (TP_o5) corresponding to the Middle Eocene Climatic optimum (MECO – Fig. 3A). A two-step lowering of about 35m of the GMSL occurs between 40 Ma (TP_o5) and 36 Ma, followed by a gradual increase of about 25m between 36 Ma and 34.5 Ma just before the Eocene-Oligocene Transition (EOT – Fig. 3A). Between 46 Ma and 34 Ma (TP_o6), the CCD is strongly oscillating with numerous deepening events of 500 to 1000 m magnitude and shoaling ones, corresponding to carbonate accumulation episodes. These oscillations in the CCD occurred during an interval indicating still high CO2 concentrations, roughly above the 750 ppmv considered as an Antarctic glaciation threshold (*62*), and marked by a relative minimum at about TP_o5 at 40 Ma (Fig. 3B,C). This first interval of the GMSL, ending by the strong deepening of about 1000m associated with a strong decrease in CO2 concentration, determines variations of a rather completely ice free Earth, at least with no major ice sheet either in southern and northern hemisphere. This is deduced first from the high GMSL, mainly above 12m (Fig. 2A), which would correspond to the mutual contribution of the Greenland and the West Antarctic ice sheets, and second from high

CO2 concentrations estimates in agreement with a CCD generally lower than 4000 m (Fig 2B,C).

The second main interval shows a completely different scenario with the GMSL varying between +30m and -80m without considering the late Quaternary interval, and much lower CCD and CO2 concentration (Fig. 2B,C). First the strong decrease in the GMSL at EOT reaches negative values of about -25m at about 33.5Ma. It is interpreted as the evidence of the first continental scale Antarctic ice sheet (first Oligocene isotope maximum - Oi1 – Fig. 2A) (*96*). After a return to values similar to present mean sea level, about +2m, between 32 Ma and 30 Ma, a new decreases of about 25m in GMSL is occurring between 29.5 Ma and 27 Ma corresponding to another continental scale Antarctic ice sheet extent labeled Oi2 (Fig. 2A). After a two-step increase in GMSL of about 40m between 27 Ma and 24 Ma, a new sharp decrease of about 40m is noticed at about 23 Ma. It corresponds to the Middle Oligocene Maximum (Mi1 – Fig. 2A), another Antarctic ice sheet wide expansion (*96*, *97*). From TP$_o$6, at 34 Ma, and 23 Ma, the CO2 concentration decreases associated with a deepening trend in the CCD down to about -4600m. From 23 Ma until about 19 Ma, GMSL shows oscillations but with lower values than present day at about -20m, whereas from 19 Ma until 17 Ma, GMSL increases by about 50m to indicate high values around +30 m above present day value (Fig. 2A). The CCD indicates about 600 m shoaling which lasted around 2.5 Myr linked to some high estimates of CO2 concentration (from paleosols, stomata) (*61*) (Fig. 2B,C). This strong increase corresponds to the Miocene Climatic optimum (MCO – Fig. 2A), between 17 Ma and TP$_o$7 at 13.9 Ma, which is the last interval during which GMSL reaches such high values (higher than +20m) above the present day ones (Fig. 2). The interval between TP$_o$7 at 13.9 Ma and 13 Ma corresponds to the Middle Miocene transition during which GMSL decreases once more significantly by about 35m. Such lowering is associated with the growth of the East Antarctic ice sheet to near its present state, remaining a perennial ice body that is thereafter impacting the Earth climate (*86*, *98*). Although GMSL remains relatively stable between 13 Ma and 12 Ma, another strong decrease, again of about 30m, occurs between TP$_o$8 at about 9 Ma and 8.5 Ma, associated with the strongest deepening recorded by the CCD, around 4800m. GMSL increases again by about 20m until 7.5 Ma to remain relatively stable until 5.5 Ma when GMSL increases by about 20m between 5.5 Ma and 3.5 Ma, corresponding to the Pliocene Climatic Optimum (PCO – Fig. 2A).

Between 3.5 Ma until TP$_o$9 at about 2.7 Ma GMSL shows a sharp decreasing trend of about 35m (Mi2a, 3, 4 – Fig. 2A) with the initiation of the development of the large northern ice sheets between 2.9 Ma (TP$_o$9a) and 2.5 Ma (TP$_o$9b – Fig. 2), especially the Laurentide ice sheet corresponding to about 50m decrease of GMSL with regards to the present day value (Fig. 2A). From TP$_o$8 at about 9 onward, CCD shows fluctuations although remaining at around 4500m with two strong deepening at about TP$_o$9a 2.9 Ma and TP$_o$9b (Fig. 2) at 2.5 Ma.

In another global sea level reconstruction, (*99*) individualized several major thresholds that agree with Miller et al (2020) reconstruction and our present analysis. Indeed they estimate the EOT global sea level drop at 34 Ma (TP$_o$6) as being of about between 30m, while previously reconstructed of 70m-80m by (*100*), and by (*54*). They also estimate this drop in global sea level being associated to a 2.5°C cooling interpreted previously as above the onset of the Antarctic ice sheet glaciation. (*99*) also identify 14 Ma (TP$_o$7) threshold as the end of the last intermittently ice free period of the Earth history of the last 40 Ma with only southern hemisphere ice sheets impacting the Earth climate. Ref. (*54*) indicates a 35m lowering at that particular transition. Indeed Ref. (*99*) indicate a slight sea level negative shift at about 10 Ma (TP$_o$8), of about 10m for (*54*), as the onset of partial or ephemeral northern Hemisphere ice bodies with 2 other sea level threshold at about 3 (about TP$_o$9a) and 2.75 (TP$_o$9b), also observed in Miller et al. (*54*). These two key dates correspond to respectively the first major iceberg calving in the Nordic Seas (*101*) and from the Laurentide ice sheet (*102*) although this interpretation was rejected by (*103*) reviewing N Atlantic ice rafted records, and rather attributing the IRD signature to Greenland and Fennoscandian glaciers. (*23*) identified the first occurrence of iceberg calving in North Atlantic at about 2.75 from the analysis of the $\delta^{18}O$ of benthic bulk carbonate in core U1308 (Supp. Fig. 3), a date identified as an abrupt transition in the RR analysis of both $\delta^{18}O$ of benthic foram and bulk carbonate (*79*). All along the past 66 Ma, GMSL has been varying between average values of +38. m ± 15 m above the present day value during the hot world interval prior TP$_o$6 at 34 Ma, and of -3.5m ± 13 m after 34 Ma until present day during the cold world interval (Tab. 2).

<u>The past 3.3 Myr.</u>

We provide here a more detailed discussion of the past 3.3 Myr. The first date, TP_o9b detected by RQA, is interpreted as corresponding to the earliest occurrence of IRD in the North Atlantic. This occurrence characterizes the presence of Northern Hemisphere coastal glaciers large enough to calve icebergs in the ocean, and the melting of these icebergs is likely to have impacted the oceanic circulation. (*103*), however, reported the occurrence of weak IRD events in the late Pliocene that they attributed mainly to Greenland and Fennoscandian glaciers. Such interpretation points to nevertheless smaller ice sheets over these regions than during the later Quaternary, when North American ice sheets were considerably larger. The interval TP_o9a, at 2.8 Ma, to RTP_o2, at 1.2 Ma, shows glacial–interglacial sea level variations of about 25–50 m below the present day. The CO2 concentrations varied between 270 ppmv and 280 ppmv during interglacials and between 210 ppmv and 240 ppmv during glacials, with a decreasing trend of about 23 ppmv over this 1.4-Myr–long interval (*104*).

The second date, RTP_o1, at 1.55 Ma, corresponds to increased amplitude in ice volume variations between glacial minima and interglacial optima. This second step shows the permanent occurrence of ice-rafted events during glacial intervals in the record (Suppl. Fig. 3), therefore an amplified relationship of climate variations with Northern Hemisphere ice sheets. The increase in IRD variability and magnitude since RTP_o1, however, shows that distinct, faster processes have to be considered than those due to slow changes in Earth's orbital parameters; see again Fig. 4.

The third date, RTP_o2, at 1.25 Ma, close to the MIS22–24 $\delta^{18}O$ optima, shows increased continental ice volume in the Northern Hemisphere (*87*), but also more stability in the East Antarctic ice sheet in Southern Hemisphere (*105*). In parallel, evidence of a major glacial pulse recorded in Italy's Po Plain, as well as in ^{10}Be-dated boulders in Switzerland, is interpreted as marking the onset of the first major glaciation in the Alps (*106*, *107*).

After RTP_o2, at1.25 Ma, the sea level changes decreased to about 70–120 m below the present day, while the CO2 concentrations varied between 250 ppmv and 320 ppmv during interglacials and between 170 ppmv and 210 ppmv during glacials (*108*). Similar variations were determined by (*109*), although pCO2 changes that occurred before the time reached by ice core records are associated with high uncertainties in both dating and values. The sawtooth pattern of the interglacial–

glacial cycles (*110*) becomes noticeable at 0.9 Ma. At about the same time, the synthetic Greenland $\delta^{18}O$ reconstruction indicates the occurrence of millennial variability expressed by DO-like events (*111*).

Finally RTP_o3, at 0.65 Ma, marks the end of the transition from the Lower and Mid-Pleistocene interval —characterized by 41-Kyr–dominated cycles and smaller 23-Kyr ones — to the Upper Pleistocene, with its 100-Kyr–dominated cycles; see Fig. 4. The sawtooth pattern of the interglacial–glacial cycles is well established during this final interval, in contradistinction with the previous, more smoothly shaped pattern that appears to follow the obliquity variations. The global ice volume is maximal, exceeding the values observed earlier in the record, especially due to the larger contribution of the Northern American ice sheets. The latter now have a bigger impact on Northern Hemisphere climate than the Eurasian ice sheets (*87*). The IRD event intensity and frequency of occurrence increase (*112*) as well (Suppl. Fig. 3), leading to the major iceberg discharges into the North Atlantic named Heinrich events (HEs); see (*113–116*),. The interval of 1 Ma – about 0.4 Ma (RTP_o4) is also the interval during which Northern Hemisphere ice sheets reached their southernmost extent (*87*). Applying Mg/Ca transfer functions, (*77*) have estimated that the past 0.4 Myr water temperatures have been the highest the past 1.2 Myr, supporting the local temperature variations deduced from the Antarctic ice cores (*117*)